Control of Iron(II) Spin States in 2,2′:6′,2″-Terpyridine Complexes through Ligand Substitution

Edwin C. Constable,*[a] Gerhard Baum,[b] Eckhard Bill,[c] Raylene Dyson,[a] Rudi van Eldik,[d] Dieter Fenske,[b] Susan Kaderli,[a] Darrell Morris,[a] Anton Neubrand,[d] Markus Neuburger,[a] Diane R. Smith,[a] Karl Wieghardt,[c] Margareta Zehnder,[a] and Andreas D. Zuberbühler[a]

Abstract: A series of 6- and 6,6″- aryl-substituted 2,2′:6′,2″-terpyridine ligands and their iron(II) complexes have been prepared. The introduction of phenyl substituents at both the 6- and 6″-positions leads exclusively to the formation of orange high-spin iron(II) complexes whilst the presence of a single 6-phenyl substituent results in spin-crossover systems. The complexes $[Fe(\mathbf{2})_2]X_2$ ($\mathbf{2}$ = 4,6-diphenyl-2,2′:6′,2″-terpyridine; X = ClO_4 or PF_6) have been studied in detail, and the solid-state X-ray structures of both the low- and high-spin forms are reported. Mössbauer spectroscopic and magnetic susceptibility measurements are reported, and the temperature and pressure dependence of the high-spin/low-spin transition have been studied. An X-ray structural study of the complex $[Fe(\mathbf{2})_2](ClO_4)_2$ is also reported; this complex is highly distorted with two very long Fe···N contacts of over 2.4 Å and is best regarded as a four-coordinate iron complex.

Keywords: iron · N ligands · magnetism · structure elucidation · supramolecular chemistry

Introduction

Transition metal ions with d^4, d^5, d^6, and d^7 electronic configurations are capable of forming complexes in either low-spin or high-spin electronic configurations depending primarily on the relative magnitudes of the ligand field and the mean spin-pairing energy. Although there are many examples of complexes that exist in one of the two ground states, there are still relatively few cases in which both high- and low-spin states are populated and coexist in thermal equilibrium. This latter is termed spin crossover, magnetic crossover, spin transition or spin equilibrium and has been extensively reviewed with particular attention focused on iron(II) complexes.[1–4] Interest in high-spin iron(II) complexes intensified when a number of metalloproteins, such as isopenicillin *N*-synthase,[5] deoxyhemerythrin[6] and ribonucleotide reductase,[7] were identified as having iron(II) centres at their active sites.

Two principal strategies have been adopted in designing ligands capable of forming spin-crossover complexes upon coordination to a six-coordinate iron(II) centre: 1) introduction of steric strain and 2) introduction of steric bulk. By far the most successful of these two methods is by the incorporation of sterically demanding substituents close to the donor atoms such that the metal-donor atom distances are longer than with the unsubstituted parent ligand. This, in turn, reduces the ligand field and will make the high-spin configuration more favourable. Many examples exist of didentate ligands in which the introduction of substituents adjacent to the donor atom(s) results in a spin crossover or high-spin complex on reaction with iron(II) salts. For example, whereas the complexes $[Fe(phen)_3]X_2$ (phen = 1,10-phenanthroline) are low-spin,[8] the introduction of a methyl substituent into the 2-position is sufficient to give spin crossover systems.[9] More recently, examples have been reported of spin crossover in supramolecular systems in which two iron(II) centres are coordinated to three didentate domains of a ligand array consisting of three symmetrical N_4 ligands[10] or one iron(II)

[a] Prof. E. C. Constable, Dr. R. Dyson, S. Kaderli, Dr. D. Morris, M. Neuburger, Dr. D. R. Smith , Prof. M. Zehnder, Prof. A. D. Zuberbühler
Institut für Anorganische Chemie der Universität Basel
Spitalstrasse 51, CH-4056 Basel (Switzerland)
Fax: +41 61-267-1015
E-mail: constable@ubaclu.unibas.ch

[b] G. Baum, Prof. D. Fenske
Institut für Anorganische Chemie der Universität Karlsruhe
Engesserstrasse, Geb.: 30 45,76128 Karlsruhe (Germany)

[c] Prof. R. van Eldik, Dr. A. Neubrand
Institut für Anorganische Chemie der Universität Erlangen-Nürnberg
Egerlandstrasse 1, 91058 Erlangen (Germany)

[d] Dr. E. Bill, Prof. K. Wieghardt
Max-Planck Institut für Strahlenchemie
D-45470 Mülheim an der Ruhr (Germany)

0947-6539/99/0502-0498 $ 17.50+.50/0 *Chem. Eur. J.* **1999**, *5*, No. 2

centre is coordinated to three didentate domains of three segmental N_5 ligands with a lanthanide ion coordinating to the three remaining tridentate domains.[11] In the latter system, the position of the spin equilibrium is controlled by the lanthanide ion.

2,2′:6′,2″-Terpyridine (tpy) forms low spin $[Fe(tpy)_2]X_2$ complexes irrespective of the counterion X,[12] and introduction of substituents at the 4′-position has no effect on the spin state.[13] We have recently shown that iron(II) complexes of disubstituted 2,2′:6′,2″:6″,2‴:6‴,2⁗:6⁗,6⁗′-sexipyridines, which may be considered as two tpy linked through the 6-position adjacent to a donor atom, are high spin in solution.[14] In this paper we describe the synthesis of a number of substituted 2,2′:6′,2″-terpyridines and their iron(II) complexes and discuss the effect of the substituents on the spin state of the iron(II) centre.

Results and Discussion

Preparation of the 2,2′:6′,2″-terpyridine ligands: Three classes of ligands were investigated: type 1 possess a single phenyl group in the 6-position and are exemplified by ligands **1** and **2**; type 2 incorporate phenyl sub-

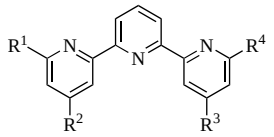

Ligand	R^1	R^2	R^3	R^4
1	Ph	H	H	H
2	Ph	Ph	H	H
3	Ph	H	H	Ph
4	Ph	Ph	Ph	Ph
5	Me	H	H	Me
6	Me	Ph	Ph	Me

stituents in both the 6- and 6″-positions (ligands **3** and **4**); in type 3 ligands the 6- and 6″-substituents of type 2 compounds are replaced with methyl groups (ligands **5** and **6**). The ligands were all prepared by using Kröhnke methodology.[15] The asymmetric type 1 ligands **1** and **2** were obtained by the reaction of the Ortoleva–King product from 6-acetyl-2,2′-bipyridine **7**[16] with Mannich salt **8** or enone **9**, respectively, in the presence of ammonium acetate (Scheme 1).

The symmetrical ligand **3** was formed from the reaction of the Mannich salt **10**, derived from 2,6-diacetylpyridine,[15] with *N*-phenacylpyridinium bromide **11** in the presence of ammonium acetate. This method afforded a significantly higher yield of **3** than that previously reported from the reaction of phenyllithium with tpy. [17] The reaction of **11** with the bischalcone of 2,6-diacetylpyridine **12**[16] in the presence of ammonium acetate afforded the 4,6,4″,6″-tetraphenyl ligand **4**. The pyridinium salt **13** is conveniently prepared from the reaction of chloroacetone with pyridine, and substitution for the *N*-phenacylpyridinium bromide in the above reactions resulted in the formation of the 6,6″-dimethyl-substituted ligands **5** and **6**. These transformations are presented in Scheme 2.

All of the ligands were isolated as colourless solids in 50–70% yield and fully characterised by standard spectroscopic and analytical techniques.

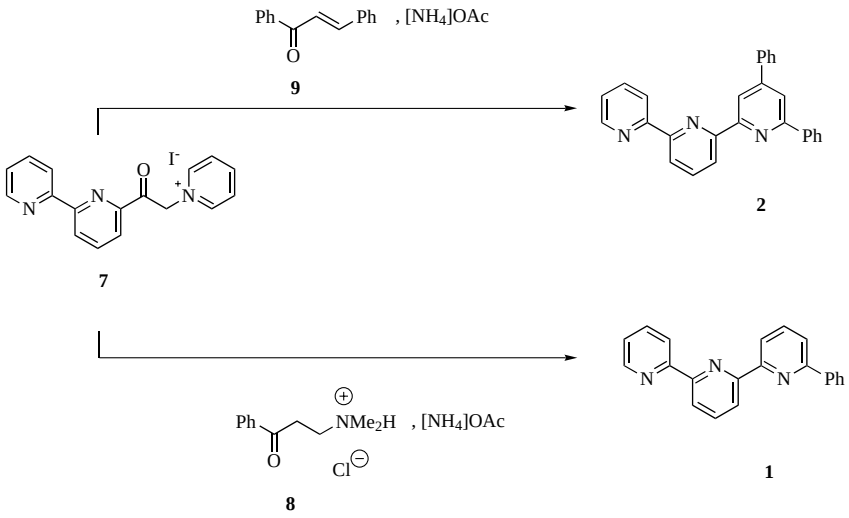

Scheme 1.

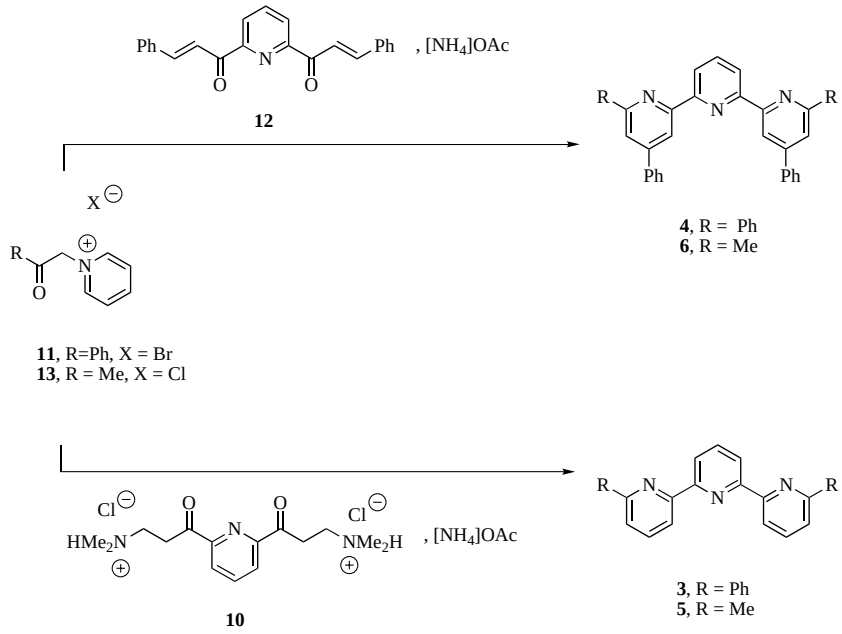

Scheme 2.

Preparation of the iron(II) complexes: The iron(II) complexes of the asymmetric type 1 ligands were obtained by the reaction of $[NH_4]_2Fe(SO_4)_2 \cdot 6H_2O$ with two equivalents of the ligand in methanolic solution. In all cases, the complexes were isolated as purple solids after the addition of a methanolic solution of ammonium hexafluorophosphate. In the case of type 2 and type 3 ligands, the complexation reactions in methanol were very slow and even after heating at reflux for several hours, solid unconverted ligand remained. For these ligands coordination was achieved by performing the reaction in ethane-1,2-diol at reflux; this produced orange solutions from which the complexes were isolated as orange solids by the addition of methanolic $[NH_4](PF_6)$ and water. The crude solids obtained from the type 1 ligands were purple, whereas those from the type 2 and type 3 ligands were orange. Recrsytallisation of the orange solids gave good quality orange crystals shown to be of stoichiometry $[FeL_2](PF_6)_2$. The behaviour of the solids obtained from the type 1 ligands was, however, unusual.

Recrystallisation of crude purple $[Fe(\mathbf{1})_2](PF_6)_2$ or $[Fe(\mathbf{2})_2](PF_6)_2$ by the diffusion of diethyl ether vapour into a purple solution of the respective compound in acetone afforded orange crystals. We originally thought that these were an iron(III) species obtained by aerial oxidation, although analysis later confirmed an $[FeL_2](PF_6)_2$ stoichiometry. Dissolving the orange crystals of $[Fe(\mathbf{1})_2](PF_6)_2$ or $[Fe(\mathbf{2})_2](PF_6)_2$ in acetone or acetonitrile afforded a purple solution from which orange crystals were again obtained upon concentration. Ion exchange of the $(PF_6)^-$ ion for perchlorate followed by vapour diffusion of diethyl ether into a solution of the respective compound in acetonitrile afforded purple crystals of $[Fe(\mathbf{1})_2](ClO_4)_2$ or $[Fe(\mathbf{2})_2](ClO_4)_2$. As will be established later, the orange species are high-spin complexes, whilst the purple compounds are low-spin. The phenomenon of changing spin state upon changing the counterion is a poorly understood consequence of crystal packing but has occasionally been observed previously.[2, 3] X-Ray quality crystals of orange $[Fe(\mathbf{2})_2](PF_6)_2$ (see Figure 6 (bottom)), purple $[Fe(\mathbf{2})_2](ClO_4)_2$ (see Figure 6 (top)) and orange $[Fe(\mathbf{3})_2](ClO_4)_2$ (see Figure 5) were obtained.

Solution studies

^{1}H NMR studies: The spin state of the iron(II) complexes was initially determined from the ^{1}H NMR spectra. The reference compound $[Fe(tpy)_2](PF_6)_2$ is purple and low spin. The high- and low-spin states are derived from the ^5D term, which splits in an octahedral field to $^5T_2$ and $^1A_1$ terms. A similar splitting occurs in the local D_{2d} symmetry of a bis(tpy) complex. A low-spin d^6 configuration with a $^1A_1$ ground term will be diamagnetic, whereas the high-spin configuration with the $^5T_2$ term will be paramagnetic. The diamagnetic complexes are expected to show resonances within the normal ^{1}H NMR spectroscopic region ($\delta = 0$ to 15), whilst the paramagnetic species are expected to exhibit paramagnetically shifted spectra with resonances extending over a large chemical shift range ($\delta = -500$ to $+500$).[18] We have demonstrated previously that the ^{1}H NMR spectra of paramagnetic cobalt(II) complexes with substituted 2,2′:6′,2″-terpyridine ligands may be used to assess the nature of solution species[19] and we have now extended this methodology to the related iron(II) complexes.

The iron(II) complexes of the type 2 (**3**, **4**) and type 3 (**5**, **6**) symmetric ligands with substituents in both the 6- and 6″-positions gave orange solutions in CD_3CN or CD_3COCD_3 with only one species present (Table 1). This species corresponds to a high-spin iron (II) complex as is evident from the ^{1}H NMR spectra which exhibit paramagnetically shifted resonances between $\delta = -20$ and $+100$. The ^{1}H NMR spectra could be assigned by comparison with each other and with the spectra of the type 1 ligand complexes. In all of the spectra, the $H^{4'}$ signal was identified from integration values as lying between $\delta = -13$ and -20. The 6-methyl and 6-phenyl resonances are broadened; the methyl resonances appear as broadened singlets at $\delta \approx -2$ and the phenyl protons are located between $\delta = +5$ and -10, although excessive broadening and overlap with solvent resonances means that it is not possible to see all five phenyl environments. In the case of the complex of **4** the signals from the phenyl rings are broadened such that they cannot all be discerned. In general, the $H^{4'}$ proton (in **3** and **5**) or the protons of the phenyl group in the 4′-position are least affected by the paramagnetic metal centre and are found between $\delta = 7$ and 15. The ^{1}H NMR spectrum of $[Fe(\mathbf{6})_2](PF_6)_2$ is shown in Figure 1a as a representative example of the high-spin iron(II) complexes. The orange solid complexes of the type 1 asymmetric ligands formed purple solutions in CD_3COCD_3 or CD_3CN. We expected the ^{1}H NMR spectra of these solutions to be characteristic of diamagnetic low-spin iron(II) species. However, the spectra were typical of paramagnetic species ($[Fe(\mathbf{1})_2](PF_6)_2$: $\delta = 107$ very broad, 54.6, 46.6, 43.1, 39.7, 37.6, 35.3, 16.1, 11.1, 7.65 (2H), 7.44 (2H), 7.23, -4.8; $[Fe(\mathbf{1})_2](PF_6)_2$: $\delta = 97$ very broad, 49.9, 42.8, 38.8, 36.6, 34.7, 32.4, 15.5, 10.2 (4H), 8.9 (2H), 8.7, 6.0 (2H), 2.5, -3.0). Figure 1b presents the ^{1}H NMR spectrum of $[Fe(\mathbf{z})_2](PF_6)_2$ in CD_3CN solution. In each case a reproducible subspectrum of a diamagnetic species was present, which we tentatively assign to the low-spin complex that is in slow exchange with the high-spin compound on the ^{1}H NMR time scale. The same subspectrum was also observed in CD_3COCD_3 solution, eliminating the possibility that the solution species contains a hypodentate didentate tpy ligand and a coordinated solvent molecule.

Table 1. ^{1}H NMR spectroscopic chemical shift data (250 MHz, 298 K) for CD_3COCD_3 solutions of paramagnetic $[FeL_2](PF_6)_2$ complexes.

L	H^3	H^4 or subst	H^5	H^6 or subst	$H^{3'}$	$H^{4'}$
3	58.6/79.3	14.4	58.6/79.3	−10.3	67.7	−20.4
					0.6	
					1.3	
					4.1	
4	59.7/80.9	9.6 *p*	9.7/80.9	1.2	69.6	−17.3
		10.0 *o*/*m*		5.0		
		13.4 *o*/*m*		[a]		
5	53.7/57.8	9.7	53.7/57.8	−2.1 Me	69.1	−17.6
6	51.9/56.9	7.3 *o*/*m*				
		8.1 *p*	51.9/56.9	−2.4 Me	69.5	−13.9
		9.0 *o*/*m*				

[a] Some resonances are broadened and not observed above the baseline.

0947-6539/99/0502-0500 $ 17.50+.50/0 *Chem. Eur. J.* **1999**, *5*, No. 2

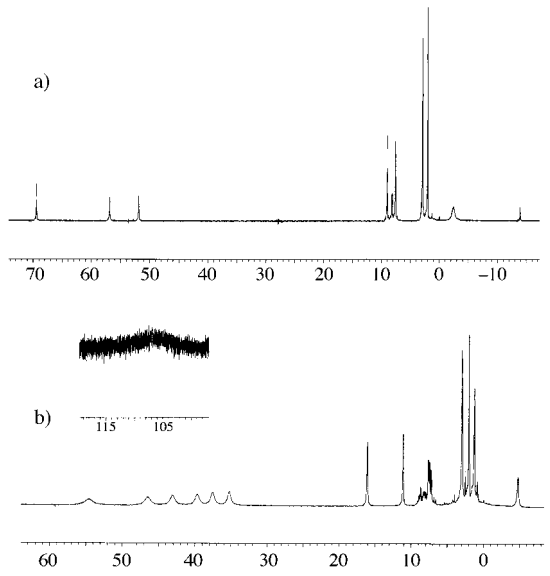

Figure 1. ^{1}H NMR spectra (250 MHz, CD_3CN solutions, 298 K) of a) $[Fe(\mathbf{6})_2](PF_6)_2$ and b) $[Fe(\mathbf{1})_2](PF_6)_2$. The inset in Figure 1b shows the downfield region.

Electronic spectra: The electronic spectra of CH_3CN solutions also provided support for the existence of both high- and low-spin species in the complexes with the type 1 ligands. The low-spin, purple, parent complex $[Fe(tpy)_2](PF_6)_2$ shows a characteristic metal-to-ligand charge transfer (MLCT) band centred at 548 nm. In contrast, the electronic spectra of the iron(II) complexes with the type 2 ligands were essentially transparent at 548 nm with the orange colour arising from a tailing into the visible of a ligand $\pi-\pi^*$ absorption at 330 nm. The iron complexes of **1** and **2** both give purple solutions in acetonitrile with absorption maxima for an MLCT band close to 550 nm and their electronic spectra appear intermediate between low-spin $[Fe(tpy)_2](PF_6)_2$ and the high-spin complexes with type 2 or type 3 ligands (Figure 2). The extinction coefficient of the MLCT band of the low-spin purple form in the visible region of the spectrum is very much larger than any absorptions of the orange form, and the visible region of the electronic spectrum is dominated by the low-spin form; the ligand $\pi-\pi^*$ transitions are expected to be similar in both high- and low-spin forms.

Temperature dependence: The equilibrium between the high-spin, orange and the low-spin, purple forms of the iron(II) complex of the type 2 ligands is expected to be temperature dependent, and we have studied the behaviour of $[Fe(\mathbf{2})_2](PF_6)_2$ in detail. Generally, the low-spin form is expected to be favoured at low temperatures, whilst the high-spin form is the high-temperature species. The changes in the electronic spectrum of a solution of $[Fe(\mathbf{2})_2](PF_6)_2$ in acetonitrile were shown to be fully reversible over the temperature range 300.0 to 323.0 K; the intensity of the 554 nm MLCT band decreases with increase in temperature (Figure 2b). In order to make more extensive studies we changed from acetonitrile (liquid range 229.3 to 354.7 K) to propionitrile (liquid range 180.0 to 370.4 K) as solvent. Monitoring the changes in absorbance intensity over the

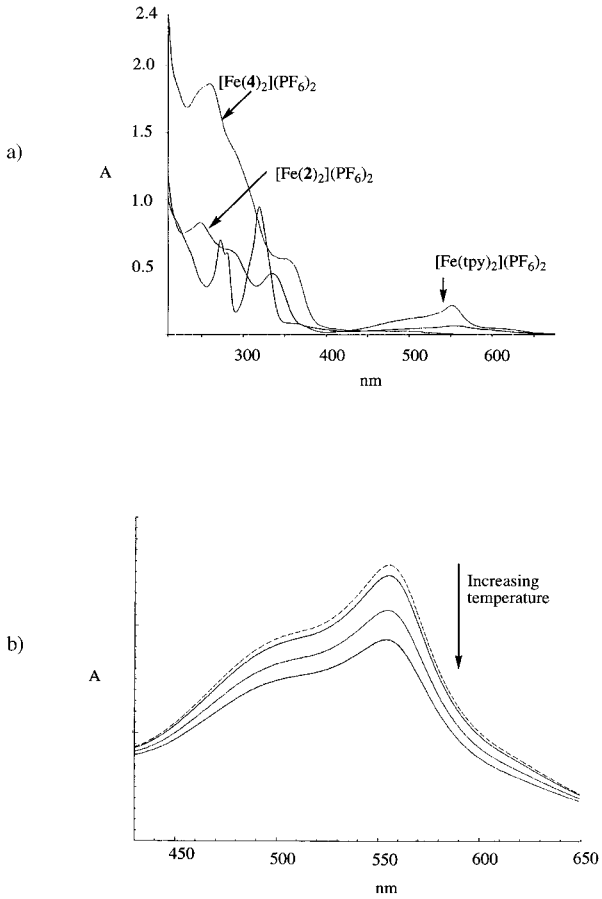

Figure 2. a) Electronic spectra of 5×10^{-5} M solutions of $[Fe(tpy)_2](PF_6)_2$, $[Fe(\mathbf{2})_2](PF_6)_2$ and $[Fe(\mathbf{4})_2](PF_6)_2$ and b) the temperature dependence of the electronic spectrum of an acetonitrile solution of $[Fe(\mathbf{2})_2](PF_6)_2$ at 300, 303, 313 and 323 K.

temperature range 180 to 320 K for a solution in propionitrile allowed the enthalpy and entropy terms associated with the spin state change to be estimated as $\Delta H = -18.7 \pm 0.1$ kJ mol^{-1} and $\Delta S = -61.8 \pm 0.4$ J K^{-1} mol^{-1} using the method of second-order globalisation.[20] Very reasonable fits with $\sigma(\text{absorbance}) < 0.01$ over the complete set of data were obtained, although the model of temperature independent spectra cannot be strictly correct. These results are in general agreement with those previously reported for another iron(II) spin-crossover system.[21] The thermodynamic data led to $\Delta G = -0.3 \pm 0.2$ kJ mol^{-1} and $K(298.15\text{ K}) = 1.13 \pm 0.09$ confirming that the system is in a genuine spin-crossover equilibrium.

Pressure dependence: The presence of electrons within the metal–ligand antibonding e_g^* orbitals which lie along the metal ligand donor atom vector in the high-spin complex result in longer Fe–N distances than in the low-spin form, in which the e_g^* orbitals are unoccupied. As a consequence, the molecular volume of the high-spin cation is expected to be greater than the low-spin form, and the equilibrium between the two spin states is expected to be pressure dependent. An acetonitrile solution of $[Fe(\mathbf{2})_2](PF_6)_2$ was placed in a pillbox of diameter 15 mm at ambient temperature and subjected to a series of six pressures, 60, 360, 660, 960, 1260 and 1560 bar and

the electronic spectra recorded at wavelengths of 336 and 554 nm, corresponding to maxima in the ligand $\pi-\pi^*$ transitions and the MLCT transition in the low-spin form, respectively. The absorption at 336 nm increased by 10.4% over the pressure range 60 to 1560 bar; the intensity increases linearly by an average of 0.021 absorbance units per 300 bar at 336 nm. This presumably represents slight changes in the absorption maximum and band width of the ligand $\pi-\pi^*$ transitions in the two forms. The MLCT absorption at 554 nm was found to increase by an average of 0.0094 absorbance units per 300 bar representing an overall absorbance increase of 37.6% over the pressure range 60–1560 bar (Figure 3). The increase in absorbance with pressure indicates the expected preference for the low-spin form with the smaller molecular volume. The changes were not fully reversible over the pressure cycle 60 to 1560 to 60 bar, with a very small amount of decomposition occurring; at both 60 and 1300 bar the absorption at 554 nm was found to decrease slightly with time.

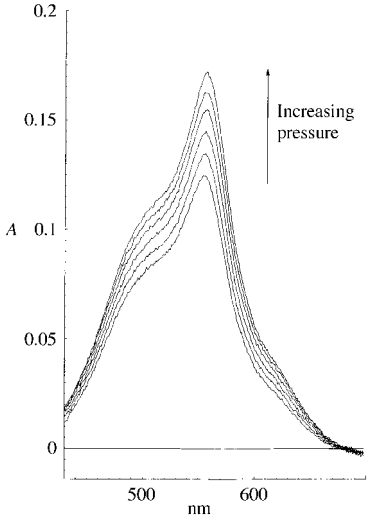

Figure 3. The pressure dependence of the electronic spectrum of an acetonitrile solution of $[Fe(\mathbf{2})_2](PF_6)_2$ at 60, 360 660, 960, 1260 and 1560 bar.

The spectral changes recorded as a function of pressure in Figure 3 can be used to estimate the volume change associated with the high-spin to low-spin conversion. In these calculations we assumed, as in the case of the temperature-dependence data, that the absorbance at 554 nm mainly originates from the low-spin state. On the basis of an equilibrium constant of 1.13 at ambient pressure for the high spin/low spin equilibrium, the increase in absorbance of 37% on increasing the pressure by 1500 atm corresponds to an increase in the equilibrium constant to 2.65. This in turn results in an overall reaction volume of $-14\ cm^3\,mol^{-1}$, which indicates that the low-spin state has a partial molar volume 14 $cm^3\,mol^{-1}$ smaller than the high-spin state. This number is in very good agreement with data reported in the literature, where typical high-spin to low-spin changes for iron(II) complexes are accompanied by volume decreases of between 4 and 16 $cm^3\,mol^{-1}$.[22–24]

Electrochemistry: All of the iron complexes discussed above are electrochemically active and exhibit a reversible iron(II)/iron(III) process together with a series of reversible or quasi-reversible ligand reductions. Data for the iron(II)/iron(III) potentials obtained from cyclic voltammetric studies of acetonitrile solutions are presented in Table 2. The iron(II)/iron(III) redox couples for the high-spin orange complexes with the type 2 and type 3 ligands lie to more positive potential than those with the type 1 ligands and are found in the range $+0.89$ to $+0.98$ V (all potentials quoted against the internal ferrocene/ferrocenium couple). This contrasts with a typical low-spin complex such as $[Fe(tpy)_2](PF_6)_2$ which exhibits an iron(II)/iron(III) couple at $+0.74$ V. The destabilisation of the iron(III) state correlates well with the longer Fe–N bonds and hence the weaker ligand field associated with the high-spin complexes. In the case of the complexes with type 1 ligands, although both high- and low-spin species are present in solution, only a single redox process corresponding to the low-spin species is observed in the region of $+0.74$ V. A comparison of the complexes with **1** and **2** indicates that the phenyl group in the 4-position is, as expected, slightly electron releasing and shifts the iron(II)/iron(III) process 20 mV to lower potential. The 6-phenyl group is expected to have a similar effect, but the redox processes for $[Fe(tpy)_2](PF_6)_2$ and $[Fe(\mathbf{1})_2](PF_6)_2$ occur at identical potentials. This presumably represents two competing effects which balance one another: a shifting to lower potential as a result of the electron-releasing phenyl substituent, and a destabilisation arising from the lengthening of Fe–N bonds with respect to tpy complexes as a result of steric interactions involving the 6-substituent (see below). Similar substituent effects are also observed in the purely high-spin species. A comparison of the complexes with **4** or **6** with those with **3** or **5** reveals that the presence of two phenyl substituents in the 4- and 4″-positions results in a lowering of the iron(II)/iron(III) process by 50 to 90 mV.

Table 2. Electrochemical potentials for the iron(II)/iron(III) process in $[FeL_2](PF_6)_2$ complexes (MeCN solvent, 0.1M $[n Bu_4N](BF_4)$ supporting electrolyte, internal ferrocene/ferrocenium reference).

L	tpy	**1**	**2**	**3**	**4**	**5**	**6**
Fe^{2+}/Fe^{3+} [V]	0.74	0.74	0.72	0.98	0.89	0.94	0.89

Solid-state species

Mössbauer spectrum and magnetic susceptibility measurements: The proof that the orange complexes were indeed high-spin iron(II) species came from studies of the solid-state materials. We will confine the discussion to the orange solid complex $[Fe(\mathbf{2})_2](PF_6)_2$, which dissolves in acetone or acetonitrile to give solutions containing both the purple and orange species. In contrast, the solid-state species only contains the orange form, which we have studied by Mössbauer spectroscopy and magnetic susceptibility measurements. The Mössbauer spectrum obtained at 80 K (Figure 4a) of $[Fe(\mathbf{2})_2](PF_6)_2$ showed a single quadrupole doublet with $\delta = 1.07\ mm\,s^{-1}$ and $\Delta E_Q \approx 1.7\ mm\,s^{-1}$, values typical for a high-spin iron(II) centre. No other iron(II) species can be detected, confirming the existence of a single solid-state species.

0947-6539/99/0502-0502 $ 17.50+.50/0 *Chem. Eur. J.* **1999**, *5*, No. 2

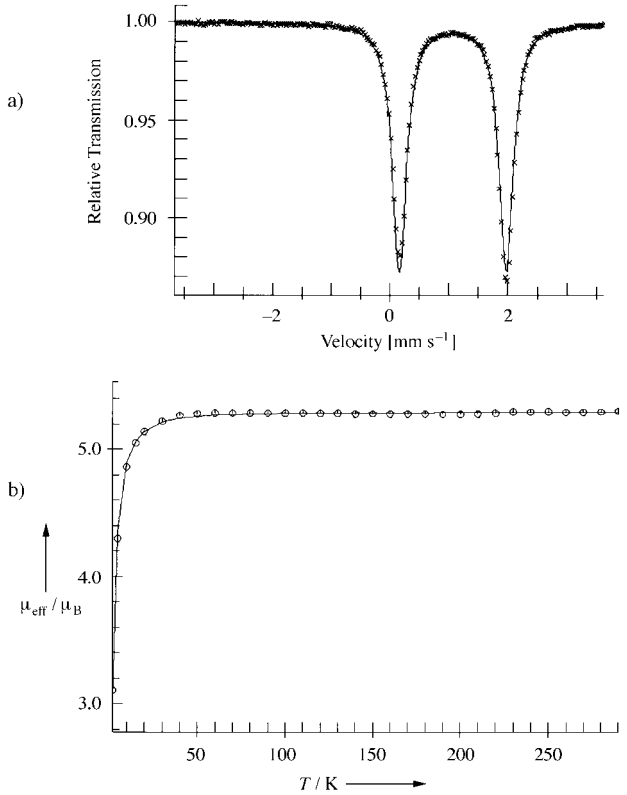

Figure 4. a) The Mössbauer spectrum of powdered orange $[Fe(\mathbf{2})_2](PF_6)_2$ at 80 K and b) the temperature dependence of the effective magnetic moment of a finely powdered mull of $[Fe(\mathbf{2})_2](PF_6)_2$ in hexane over the temperature range 4 to 290 K.

The magnetic susceptibility of the orange crystals of $[Fe(\mathbf{2})_2](PF_6)_2$ was determined over the temperature range 4 to 290 K using a SQUID magnetometer. Initial measurements indicated anomalous behaviour with a pronounced susceptibility maximum at 20 K, behaviour that was repeatable with crystalline samples from different batches of the complex. This proved to be an artefact arising from the combined effects of medium-range intermolecular interactions within the lattice and orientation of the crystals in the magnetic field. This effect has been observed previously[21] and was eliminated by grinding the solid and mixing it with a drop of hexane before freezing. Finely powdering the sample reduced but did not eliminate the effect at 20 K. Figure 4b presents the susceptibility data over the temperature range 4 to 290 K for the fine powder in hexane, after a diamagnetic correction for complex in the hexane matrix has been applied, and shows typical Curie–Weiss behaviour with a magnetic moment of 5.3 μ_B over the temperature range 290 to 40 K. This value is typical for a high-spin iron(II) ($S = 2$) ion in a complex showing distortion from ideal octahedral geometry. Below 40 K there is a reduction in magnetic moment down to a value of 3.1 μ_B at 4 K. This behaviour is associated with zero-field splitting of the spin quintet state. A spin-Hamiltonian simulation of the experimental data (solid line) yielded a zero-field parameter $|D| = 7.9$ cm^{-1} and a g value of 2.16, which is in the usual range for octahedral iron(II) complexes. To conclude, in the solid state, all of the orange complexes are high spin iron(II) species.

Heating crystals of the purple, low-spin complex $[Fe(\mathbf{2})_2](ClO_4)_2 \cdot Me_2CO$ resulted in loss of solvent in the range 80–100 °C and the formation of a dark coloured powder. On the one occasion that the experiment was attempted, the complex underwent explosive decomposition in the region of 120 °C.

X-Ray crystallographic studies

Finally, we have determined the solid-state X-ray structures of the representative complexes, orange high-spin $[Fe(\mathbf{2})_2](PF_6)_2 \cdot 2Me_2CO$, purple low-spin $[Fe(\mathbf{2})_2](ClO_4)_2 \cdot Me_2CO$ and orange high spin $[Fe(\mathbf{3})_2](ClO_4)_2 \cdot MeCN \cdot H_2O$. Crystal data for the three structural determinations are presented in Table 3. We commence the discussion by considering the parent, low-spin $[Fe(tpy)_2]^{2+}$ cation; two structural studies of this cation together with one of a related complex with propyloxy substituents in the 5 and 5″-positions have been reported.[25–27] In all cases comparable Fe–N distances are the same (within esds) and show an average Fe–$N_{terminal}$ distance of 1.981 Å and an average Fe–$N_{central}$ distance of 1.885 Å, with an average $N_{terminal}$-Fe-$N_{central}$ bite angle of 80.97°.

The $[Fe(tpy)_2]^{2+}$ ion may now be compared with the cation present in orange, high-spin $[Fe(\mathbf{3})_2](ClO_4)_2 \cdot MeCN \cdot H_2O$, the structure of which is presented in Figures 5 (top) and 5 (bottom) and selected geometrical data are presented in Table 4. There are a number of features of note; there is extensive intramolecular π stacking and as a result there is a relatively great deviation of the 2,2′:6′,2″-terpyridine system from planarity although the individual aromatic rings are planar. The two ligands embrace each other tightly in a tennis-ball structure. The terminal pyridine rings form two sets. One set of two rings is twisted with dihedral angles of 7 to 8°, whilst the other has dihedral angles of 25 to 26° with respect to the central rings; the phenyl substituents are similarly twisted with dihedral angles to the terminal pyridine rings of 38 to 52°. The consequence is a highly distorted and compressed structure. All of the Fe–N distances are larger than in the low-spin complexes. However, the two terminal pyridine rings behave very differently to one another. The rings with the smaller dihedral angle show Fe–N distances of 2.205(3) and 2.208(3) Å, whilst the central rings show the expected shorter distances of 2.089(3) and 2.092(3) Å. In contrast, the terminal pyridine rings with the large dihedral angle show very long Fe···N distances of 2.436 and 2.456 Å which cannot be regarded as fully bonding. Additional support for this claim comes from the angle of the Fe···N vector with the plane of the pyridine ring, which is found to be 143 to 144° for these two terminal rings instead of the expected 180°. The precise description of the coordination geometry in this complex is semantic. It seems to lie somewhere between a highly distorted six-coordinate complex and a four-coordinate compound with two additional weak interactions. The phenyl rings are π-stacked (approximately coplanar, interplanar distances 3.2 to 3.6 Å) with one central and one terminal ring of the other ligand. The terminal pyridine rings with the 25 to 26° dihedral angles are mutually π-stacked. All of the data are consistent with the adoption of the high-spin configuration, the various steric interactions within the ligand array force the long Fe–N distances and a correspondingly weak ligand field.

Table 3. Crystal data and parameters for $[Fe(\mathbf{2})_2](PF_6)_2 \cdot 2Me_2CO$, $[Fe(\mathbf{2})_2](ClO_4)_2 \cdot Me_2CO$ and $[Fe(\mathbf{3})_2](PF_6)_2 \cdot MeCN \cdot H_2O$.

	$[Fe(\mathbf{2})_2](PF_6)_2 \cdot 2Me_2CO$	$[Fe(\mathbf{2})_2](ClO_4)_2 \cdot Me_2CO$	$[Fe(\mathbf{3})_2](ClO_4)_2 \cdot MeCN \cdot H_2O$
formula	$C_{60}H_{50}FeN_6P_2F_{12}O_2$	$C_{57}H_{44}FeN_6Cl_2O_9$	$C_{56}H_{43}FeN_7Cl_2O_9$
mass	1232.87	1083.77	1084.76
colour	orange	purple	orange
crystal system	triclinic	monoclinic	monoclinic
space group	$P\bar{1}$	$P2_1/c$	$P2_1/c$
a [Å]	14.029(2)	20.886(4)	10.544(1)
b [Å]	14.542(5)	13.374(3)	24.656(3)
c [Å]	14.721(4)	17.810(4)	19.114(3)
α [°]	73.037(24)	90	90
β [°]	79.507(20)	97.82(3)	103.709(8)
γ [°]	79.181(19)	90	90
Z	2	4	4
F(000)	1264	2240	2240
ρ [g cm^{-3}]	1.46	1.46	1.49
μ [mm^{-1}]	3.50	0.48	4.11
diffractometer	Enraf-Nonius CAD4	IPDS Image Plate, Stoe	Enraf-Nonius CAD4
crystal size [mm]	$0.18 \times 0.52 \times 0.60$	$0.1 \times 0.1 \times 0.05$	$0.18 \times 0.32 \times 0.38$
temperature [K]	293	193	223
radiation [λ ([Å])]	$Cu_{K\alpha}$ (1.54178)	$Mo_{K\alpha}$ (0.71073)	$Cu_{K\alpha}$ (1.54180)
scan type	ω-2θ		ω-2θ
θ_{max} [°]	58.53	25.97	77.50
absorption correction	empirical	none	empirical
no. measured reflns.	8291	16664	8781
no. independent reflns.	7923	8014	8444
no. reflns in refinement	3 056, $I > 3\sigma(I)$	4 583, $I > 2\sigma(I)$	6 280, $I > 3\sigma(I)$
no. of variables	748	694	677
final R	0.0735	0.0604 ($I > 2s(I)$)	0.0562
final Rw	0.0780	0.1317 (wR2, $I > 2\sigma(I)$)	0.0685
weighting	Chebychev polynomial[a]	[d]	Chebychev polynomial[a]
Last max/min [e Å^{-3}]	0.58/ − 0.41	0.463/ − 0.722	0.56/ − 0.64
programs used	SIR92,[b] CRYSTALS[c]	SHELXS-86,[e] SHELXL-93[f]	SIR92,[b] CRYSTALS[c]

[a] J. R. Carruthers, D. J. Watkin, *Acta Crystallogr. Sect. A,* **1979**, *35*, 698. [b] SIR92, C. Giacovazzo, University of Bari, **1992**. [c] CRYSTALS, Issue 9, D. Watkin, Chemical Crystallography Laboratory, Oxford, **1990**. [d] $w = 1/[\sigma^2 (F_o^2) + (0.0739P)^2 + 0.0000P]$ where $P = (F_o^2 + 2F_c^2)/3$. [e] G. M. Sheldrick, SHELXS-86, Universität Göttingen, **1986**. [f] G. M. Sheldrick, SHELXS-93, Universität Göttingen, **1997**.

One of the two enantiomeric cations present in low-spin, purple $[Fe(\mathbf{2})_2](ClO_4)_2 \cdot Me_2CO$ is presented in Figure 6 (top) and relevant geometrical data are listed in Table 4. The structure is that of a distorted octahedron. As we have previously noted, the introduction of a single substituent into the 6-position of a tpy ligand results in the formation of chiral $\{M(L)_2\}$ complexes,[19] and the lattice contains equal numbers of cations with Δ and Λ configurations. The two $Fe-N_{terminal}$ bonds to the unsubstituted terminal rings exhibit normal short distances of 1.997(5) and 1.996(5) Å as do the $Fe-N_{central}$ bonds of 1.891(5) and 1.878(4) Å, all of which are slightly longer than, but comparable with, those in low-spin $[Fe(tpy)_2]^{2+}$ salts. The Fe–N distances to the rings bearing the phenyl substituents are slightly lengthened at 2.054(5) and 2.048(4) Å but still typical of the low-spin complex and show none of the gross distortions observed in $[Fe(\mathbf{3})_2](ClO_4)_2 \cdot MeCN \cdot H_2O$. The bite angles are all of the order of 80°. Each of the tpy units is essentially planar, with the 6-phenyl and 4-phenyl rings twisted at 97 and 24° with respect to the bonded pyridine, respectively. Once again, there is π stacking within the cation and the 6-phenyl group lies approximately coplanar (interplanar angle 7–8°) with, and 3.2 to 3.5 Å above, the central pyridine ring of the other ligand. In conclusion, the structure of the $[Fe(\mathbf{2})_2]^{2+}$ ion in the purple salts is typical of a low-spin species. Although not octahedral, the degree of distortion from the ideal geometry is small, as assessed by the N-Fe-N angles between opposite vertices, which all lie in the range 160 to 169°.

One of the two enantiomeric cations present in high-spin, orange $[Fe(\mathbf{2})_2](PF_6)_2 \cdot 2Me_2CO$ is presented in Figure 6 (bottom) and relevant geometrical data are listed in Table 4. The structure is once again that of a distorted octahedron. The two $Fe-N_{terminal}$ bonds to the unsubstituted terminal rings exhibit long distances of 2.275(7) and 2.266(7) Å reminiscent of those in high-spin $[Fe(\mathbf{3})_2](ClO_4)_2 \cdot MeCN \cdot H_2O$ as are the $Fe-N_{central}$ distances of 2.093(8) and 2.107(8) Å. The Fe–N distances to the ring bearing the phenyl substituents are lengthened with respect to the low-spin form, but closely resemble those to the unsubstituted pyridine at 2.255(7) and 2.232(7) Å and apparently typical of the high-spin cation. The pattern of Fe–N bonds is inverted with respect to the low-spin complex $[Fe(\mathbf{2})_2](ClO_4)_2 \cdot Me_2CO$; in the low-spin compound the Fe–N bonds to the substituted ring are longer than those to the unsubstituted pyridine rings, whereas in the high-spin compound the Fe–N bonds to the substituted rings are shorter. The bite angles are smaller than in the low-spin cation, lying in the range 73 to 75°, as expected for the longer Fe–N distances. None of the massive distortion of the complex with ligand **3** is observed. Each of the tpy units is bowed, with the 6-phenyl and 4-phenyl rings twisted at 46 and 35° with respect to the bonded pyridine rings, respectively. There is no significant π-stacking within the cation on this

0947-6539/99/0502-0504 $ 17.50+.50/0 *Chem. Eur. J.* **1999**, *5*, No. 2

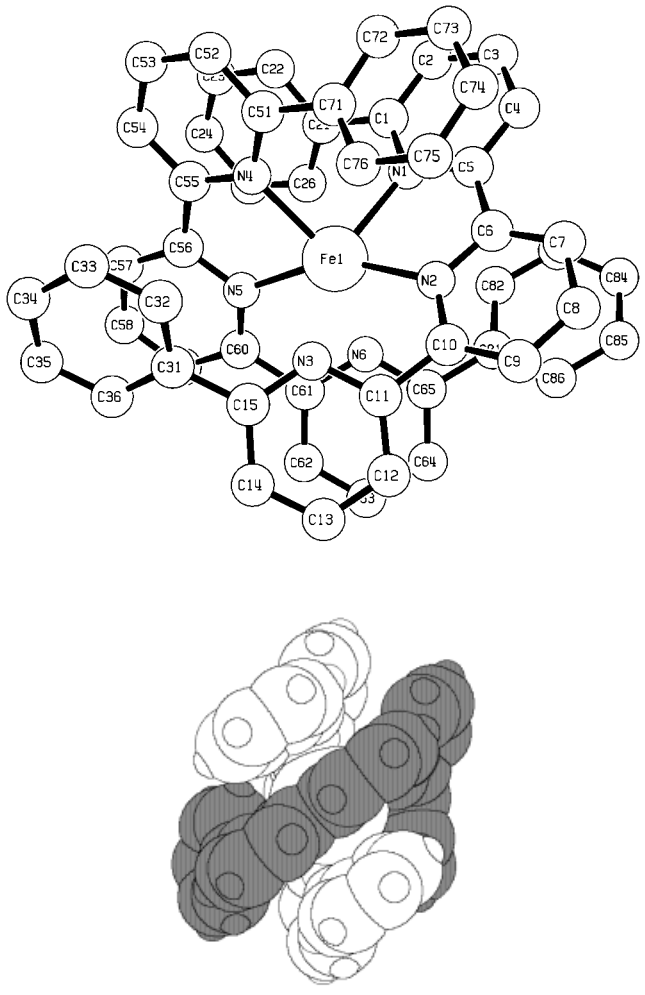

Figure 5. The crystal and molecular structure of the cation $[Fe(\mathbf{3})_2]^{2+}$ present in $[Fe(\mathbf{3})_2](ClO_4)_2 \cdot MeCN \cdot H_2O$ showing the numbering scheme adopted (top), hydrogen atoms omitted for clarity and (bottom) space-filling representation showing how the two ligands are intimately intertwined.

occasion, with the 6-phenyl group making an interplanar angle of 25° with the central pyridine ring of the other ligand. The structure of the $[Fe(\mathbf{2})_2]^{2+}$ ion in the orange salts is typical of a high-spin species. The degree of distortion from the ideal geometry is greater than in the low-spin form, as assessed by the N-Fe-N angles between opposite vertices, which lie in the range 147 to 154°.

The detailed structural studies beg the question as to whether the factors leading to high- or low-spin species may be quantified. The structural data for the high- and low-spin forms of the $[Fe(\mathbf{2})_2]^{2+}$ ion confirm that the high-spin form is larger than the low-spin form, as predicted on the basis of ligand field effects and as found experimentally from the studies of the pressure dependence of the electronic spectra and speciation. Figure 7 presents the best overlay of the high-spin (grey) and low-spin (white) forms of the $[Fe(\mathbf{2})_2]^{2+}$ ion. Although the generally larger dimensions of the high-spin form may be discerned by a careful analysis, the most striking feature is the high degree of overlap of the central rings and the unsubstituted terminal rings, but the high conformational differences associated with the substituted terminal pyridine ring.

In the case of $[Fe(\mathbf{2})_2](ClO_4)_2 \cdot Me_2CO$ there are a number of close contacts within the lattice and a large number of C–H···O hydrogen bonds between aromatic C–H bonds and perchlorate oxygen atoms with H···O contacts of 2.4–2.6 Å may be characterised. In addition, there are hydrogen-bonding interactions involving the oxygen of the acetone molecule in the lattice. The most significant of these are between C(15)–H(15) and C(18)–H(18) and the acetone in the symmetry-related $x, -1+y, z$ position, which exhibit C···O contacts of 3.428(9) and 3.351(8) Å and H···O contacts of 2.496(9) and 2.405(8) Å, respectively. The H(18)···O contact is the closest non-bonded contact other than those within the cation itself. A similar pattern exists within the lattice of $[Fe(\mathbf{2})_2](PF_6)_2 \cdot 2Me_2CO$, the shortest

Table 4. A comparison of bond lengths [Å] and bond angles [°] within the coordination spheres of the cations in $[Fe(\mathbf{2})_2](ClO_4)_2 \cdot Me_2CO$, $[Fe(\mathbf{2})_2](PF_6)_2 \cdot 2Me_2CO$ and $[Fe(\mathbf{3})_2](ClO_4)_2 \cdot MeCN \cdot H_2O$.

$[Fe(\mathbf{2})_2](ClO_4)_2 \cdot Me_2CO$		$[Fe(\mathbf{2})_2](PF_6)_2 \cdot 2Me_2CO$		$[Fe(\mathbf{3})_2](ClO_4)_2 \cdot MeCN \cdot H_2O$	
Fe1–N(1)	1.997(5)	Fe(1)–N(1)	2.275(8)	Fe(1)–N(1)	2.205(3)
Fe1–N(2)	1.891(5)	Fe(1)–N(2)	2.093(8)	Fe(1)–N(2)	2.089(3)
Fe1–N(3)	2.054(5)	Fe(1)–N(3)	2.255(7)	Fe(1)–N(4)	2.208(3)
Fe1–N(4)	1.996(5)	Fe(1)–N(4)	2.266(7)	Fe(1)–N(5)	2.092(3)
Fe1–N(5)	1.878(4)	Fe(1)–N(5)	2.107(8)	Fe(1)···N(3)	2.436
Fe1–N(6)	2.048(4)	Fe(1)–N(6)	2.232(7)	Fe(1)···N(6)	2.456
N(1)-Fe1-N(2)	80.3(2)	N(1)-Fe(1)-N(2)	73.1(3)	N(1)-Fe(1)-N(2)	75.9(1)
N(1)-Fe1-N(3)	160.90(17)	N(1)-Fe(1)-N(3)	147.4(3)	N(1)-Fe(1)-N(4)	89.3(1)
N(1)-Fe1-N(4)	90.44(19)	N(1)-Fe(1)-N(4)	87.8(3)	N(2)-Fe(1)-N(4)	125.4(1)
N(1)-Fe1-N(5)	89.8(2)	N(1)-Fe(1)-N(5)	88.0(3)	N(1)-Fe(1)-N(5)	125.3(1)
N(1)-Fe1-N(6)	92.23(19)	N(1)-Fe(1)-N(6)	98.8(3)	N(2)-Fe(1)-N(5)	152.8(1)
N(2)-Fe1-N(3)	80.7(2)	N(2)-Fe(1)-N(3)	75.6(3)	N(4)-Fe(1)-N(5)	75.9(1)
N(2)-Fe1-N(4)	93.90(18)	N(2)-Fe(1)-N(4)	88.6(3)		
N(2)-Fe1-N(5)	168.4(2)	N(2)-Fe(1)-N(5)	154.8(3)		
N(2)-Fe1-N(6)	105.73(17)	N(2)-Fe(1)-N(6)	122.9(3)		
N(3)-Fe1-N(4)	91.67(19)	N(3)-Fe(1)-N(4)	100.5(3)		
N(3)-Fe1-N(5)	109.3(2)	N(3)-Fe(1)-N(5)	124.6(3)		
N(3)-Fe1-N(6)	92.12(19)	N(3)-Fe(1)-N(6)	90.5(3)		
N(4)-Fe1-N(5)	80.12(18)	N(4)-Fe(1)-N(5)	73.8(3)		
N(4)-Fe1-N(6)	160.36(18)	N(4)-Fe(1)-N(6)	148.4(3)		
N(5)-Fe1-N(6)	80.43(17)	N(5)-Fe(1)-N(6)	75.6(3)		

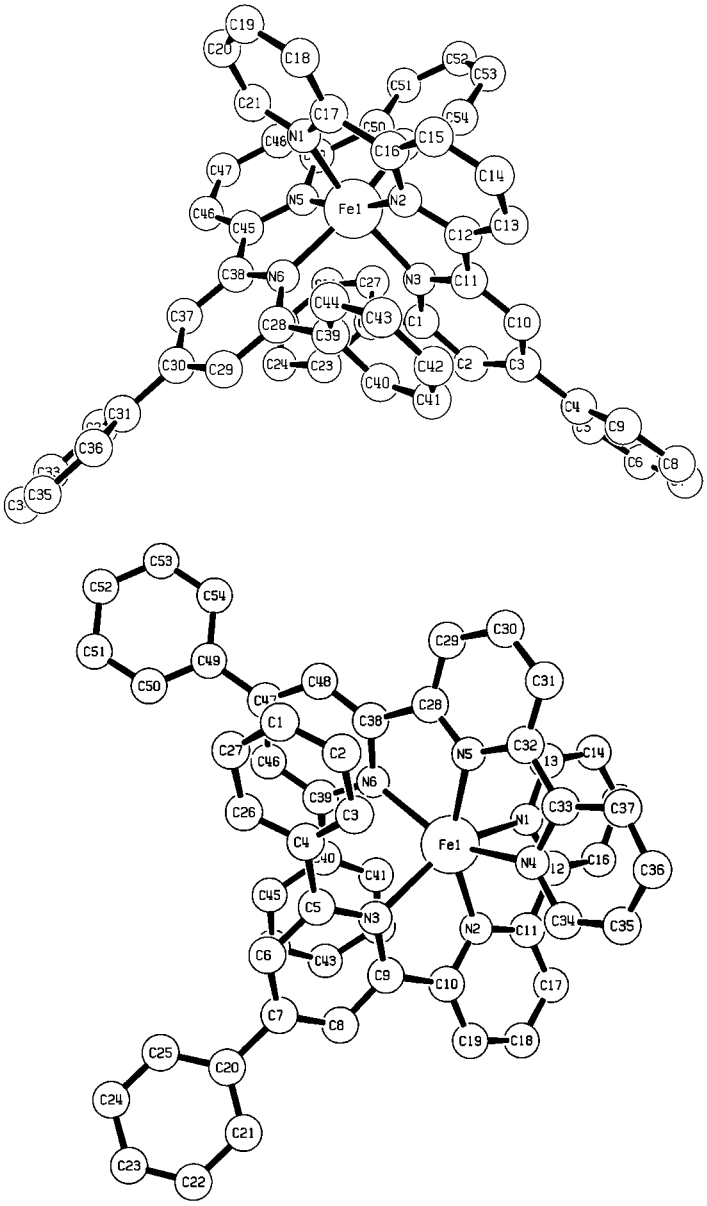

Figure 6. The crystal and molecular structure of one of the enantiomeric the cations showing the numbering scheme adopted, hydrogen atoms omitted for clarity, present in (top) low-spin, purple $[Fe(\mathbf{2})_2](ClO_4)_2 \cdot Me_2CO$ and (bottom) high-spin, orange $[Fe(\mathbf{2})_2](PF_6)_2 \cdot 2Me_2CO$.

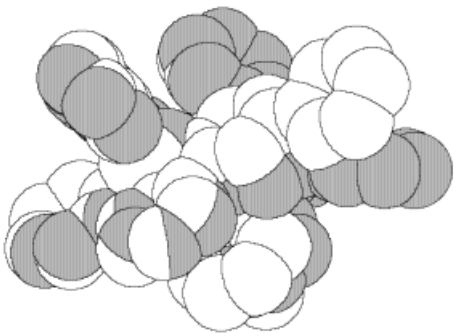

Figure 7. Minimised overlay of low-spin $[Fe(\mathbf{2})_2]^{2+}$ (white) and high-spin $[Fe(\mathbf{2})_2]^{2+}$ (grey) ions.

contact of which is between C(8)–H(81) and one of the acetone molecules in the $-x, -y, 2-z$ symmetry. In this case the C···O contact is 3.366(14) Å and the H···O contact is 2.4085 Å, respectively. The significance of these interactions in determining the final spin state is at present unclear.

Conclusion

We have shown that the introduction of two substituents into the 6- and 6″-positions of a 2,2′:6′,2″-terpyridine results in the formation of high-spin $[FeL_2]^{2+}$ species. In the case of the complex with ligand **3** the coordination geometry is highly distorted and lies between a coordination number of 4 and 6. When a single substituent is introduced into the 6-position, complexes are obtained in which the high- and low-spin forms are in thermal equilibrium at room temperature. We are currently trying to fine tune these effects.

Experimental Section

Infrared spectra were recorded on Mattson Genesis Fourier-transform spectrophotometers with samples in compressed KBr discs. ^{1}H NMR spectra were recorded on a Bruker AM 250 MHz spectrometer. UV/Vis measurements were performed by using a Perkin Elmer Lambda 19 spectrophotometer and were recorded in acetonitrile at a concentration of 5×10^{-5} M. Time of flight (MALDI) spectra were recorded by using a PerSeptive Biosystems Voyager-RP Biospectrometry Workstation. Electrochemical measurements were performed with an Amel model 553 potentiostat connected to an Amel model 567 function generator and an Amel model 560/A interface or an Eco Chemie Autolab PGSTAT 20 system using platinum bead working and auxiliary electrodes with an Ag/AgCl electrode as reference. The experiments were conducted by using purified acetonitrile as solvent and 0.1 M $[Bu^n_4N]BF_4$ as supporting electrolyte; ferrocene was added at the end of each experiment as an internal reference.

Magnetic susceptibilities of the polycrystalline samples were recorded on a SQUID magnetometer (MPMS, Quantum Design) in the temperature range 2–300 K with an applied field of 1 T. Experimental data were corrected for underlying diamagnetism with Pascal's constants ($\chi_{Dia} = 295 \times 10^{-6}$ cm^3 mol^{-1}). Mössbauer spectra were recorded on an alternating constant–acceleration spectrometer. The minimum experimental line width was 0.24 mm s^{-1} full width at half maximum. The sample temperature was kept constant in a Variox cryostat (Oxford Instruments). The Mössbauer source was about 1 GBq ^{57}Co in Rh matrix. Isomer shifts are given relative to α-Fe at room temperature.

For the temperature-dependence experiments, UV/Vis spectra were obtained in propionitrile with a SFL-21 variable temperature stopped flow unit (Hi-Tech) connected to a Tidas 16 diode array spectrometer (J and M, 507 diodes). Two series of 14 spectra were taken between 182.6 and 312.2 K. The concentration of complex (2.04×10^{-4} M at 298 K) was adjusted to take thermal expansion of the solvent into account using $\rho(\text{g cm}^{-3}) = 1.069 - (9.8 \times 10^{-4} T(\text{K}))$. Each series was subjected to second-order global analysis assuming the high-spin form of the complex to be nonabsorbing relative to the low-spin form above 450 nm (325 diodes), allowing a direct calculation of reaction enthalpy and reaction entropy as the adjustable parameters. Final results are weighted means of these two independent series.

Pressure effects on the spectra were monitored by using a Shimadzu UV 2101 instrument equipped with a home-made high-pressure cell. A pillbox type cuvette was used and the temperature was held constant to ± 0.1 K during all the measurements of the pressure cycle.[28, 29]

6-Acetyl-2,2′-bipyridne **7**,[16] the bis-chalcone **12**[30] and the bis-Mannich salt **10**[15] were prepared by the literature methods. The Mannich salt of acetophenone **8** was prepared by standard methods. Chalcone **9** was used as supplied by Aldrich. The salt **13** was prepared as a white solid from the

0947-6539/99/0502-0506 $ 17.50+.50/0 *Chem. Eur. J.* **1999**, *5*, No. 2

reaction of chloroacetone with pyridine in diethyl ether; **11** was purchased from Aldrich.

6-Phenyl-2,2′:6′,2″-terpyridine (**1**): A mixture of **7** (150 mg, 0.38 mmol), **8** (81 mg, 0.38 mmol) and anhydrous ammonium acetate (1.5 g, excess) in MeOH (10 mL) was heated to reflux for 18 h. After cooling the mixture, the resulting precipitate was filtered off and recrystallised from EtOH to give **1** as an off-white solid (78 mg, 66 %); m.p. 206–207 °C; ^{1}H NMR ($CDCl_3$, 250 MHz): $\delta = 7.33$ (m, 1H, $H^{5''}$), 7.51 (m, 3H, $H^{m,p}$), 7.80 (dd, $J =$ 7.8, 1,0 Hz, 1H, H^5), 7.87 (td, $J = 6.8$, 1.5 Hz, 1H, $H^{4''}$), 7.93 (t, $J = 7.8$ Hz, 1H, $H^{4'}$), 7.98 (t, $J = 7.8$ Hz, 1H, H^4), 8.18 (m, 2H, H^0), 8.47 (dd, $J = 7.8$, 1.4 Hz, 1H, $H^{5'}$), 8.59 (dd, $J = 7.8$, 1 Hz, 1H, $H^{3''}$), 8.67 (m, 3H, $H^{3,6,3'}$); ^{13}C NMR ($CDCl_3$, 61 MHz): $\delta = 119.4$, 120.3, 121.0, 121.2, 121.3, 123.7, 127.0 (2C), 128.7 (2C), 129.0, 136.9, 137.6, 137.8, 139.4, 149.1, 155.3, 155.6, 155.8, 156.3, 156.5; IR (KBr): $\tilde{\nu} = 3053$w, 1565s, 1473m, 1442m, 1424s, 1375m, 1265m, 1107w, 1086m, 1073m, 1042w, 1026m, 987m, 815m, 783m, 758s, 686m, 654m, 633m, 619m, 586m cm^{-1}; TOF-MS: *m/z*: 309 $[M]^+$, 332 $[M+Na]^+$, 348 $[M+K]^+$.

4,6-Diphenyl-2,2′:6′,2″-terpyridine (**2**): A mixture of **7** (150 mg, 0.38 mmol), **9** (80 mg, 0.38 mmol) and anhydrous ammonium acetate (1.5 g, excess) in MeOH (10 mL) was heated at reflux for 18 h. After cooling the mixture, the beige precipitate was filtered off and recrystallised from EtOH to give **2** as an off white solid (100 mg, 71 %); m.p. 108–110 °C; ^{1}H NMR ($CDCl_3$, 250 MHz): $\delta = 7.34$ (ddd, $J = 1.1$, 4.8, 7.5 Hz, 1H, $H^{5''}$), 7.42–7.60 (m, 6H, H^m,$H^{m'}$,H^p,$H^{p'}$), 7.84 (m, 2H, $H^{o'}$), 7.87 (m, 1H, $H^{4''}$), 7.98 (d, $J = 1.5$ Hz, 1H; H^5), 8.00 (t, $J = 7.8$ Hz, 1H, $H^{4'}$), 8.24 (m, 2H; H^o), 8.49 (dd, $J = 0.8$, 7.8 Hz, 1H, $H^{5'}$), 8.65 (d, $J = 8.0$ Hz, 1H, $H^{3''}$), 8.72 (m, 1H, $H^{6''}$), 8.73 (m, 1H, $H^{3'}$), 8.80 (d, $J = 1.5$ Hz, 1H, H^3); ^{13}C NMR ($CDCl_3$, 61 MHz): $\delta = 117.7$, 118.7, 121.1, 121.2, 121.5, 123.7, 127.1 (2C), 127.3 (2C), 128.8, 129.0, 129.1 (4C), 136.9, 137.8, 139.2, 139.5, 149.1, 150.3, 155.3, 155.6, 156.3, 156.4, 157.1; IR (KBr): $\tilde{\nu} = 3056$w, 3033w, 1597m, 1578s, 1561s, 1548s, 1496m, 1475m, 1456w, 1447w, 1434w, 1424m, 1400s, 1266w, 1077w, 785s, 764s, 757s, 693s, 645m, 631w, 620m 586m cm^{-1}; EI-MS: *m/z*: 385 $[M^+]$; $C_{27}H_{19}N_3 \cdot 0.5\,H_2O$ (345); elemental analysis calcd (%): C 82.2, H 5.1, N 10.65; found: C 82.0, H 5.0, N 10.7.

6,6″-Diphenyl-2,2′:6′,2″-terpyridine (**3**): A mixture of **10** (100 mg, 0.29 mmol), **11** (190 mg, 0.60 mmol) and anhydrous ammonium acetate (1.5 g, excess) in MeOH (10 mL) was heated at reflux for 18 h. After cooling the mixture, the precipitate was filtered off and recrystallised from EtOH to give **3** as an off-white solid (56 mg, 56 %); m.p. 205–206 °C; ^{1}H NMR ($CDCl_3$, 250 MHz): $\delta = 7.50$ (m, 6H, $H^{m,p}$), 7.80 (d, $J = 7.8$ Hz, 2H, H^5), 7.94 (t, $J = 7.8$ Hz, 2H, H^4), 8.01 (t, $J = 7.8$ Hz, 1H, $H^{4'}$), 8.18 (m, 4H, H^o), 8.62 (d, $J = 7.8$ Hz, 2H, $H^{3'}$), 8.70 (d, $J = 7.8$ Hz, 2H, H^3); ^{13}C NMR ($CDCl_3$, 61 MHz) $\delta = 119.4$ (2C), 120.3 (2C), 121.3 (2C), 127.0 (2C), 128.8 (2C), 129.0 (1C), 137.6 (2C), 137.8 (1C), 139.4 (2C), 155.5 (2C), 156.0 (2C), 156.5 (2C); IR (KBr): $\tilde{\nu} = 3053$w, 3035w, 1567s, 1431s, 1365w, 1267w, 1110w, 1089w, 1075m, 1023w, 989w, 804m, 762s, 695m, 636m cm^{-1}; TOF-MS: *m/z*: 345 $[M]^+$, 408 $[M+Na]^+$, 424 $[M+K]^+$; $C_{27}H_{19}N_3$ (345); elemental analysis calcd: C 84.1, H 5.0, N 10.9; found: C 83.9, H 5.3, N 10.8.

4,6,4″,6″-Tetraphenyl-2,2′:6′,2″-terpyridine (**4**): A mixture of **12** (230 mg, 0.66 mmol), **11** (370 mg, 1.34 mmol), and anhydrous ammonium acetate (3.1 g, excess) was heated at reflux in MeOH (20 mL) for 16 h. After leaving the mixture to stand at 0 °C for 24 h, the cream precipitate was filtered off, recrystallised from EtOH and dried over P_4O_{10} to give **4** as an off-white solid (250 mg, 71 %); m.p. 261–263 °C; ^{1}H NMR ($CDCl_3$, 250 MHz): $\delta = 7.42$–7.60 (m, 12H, H^m,$H^{m'}$,H^p,$H^{p'}$), 7.86 (m, 4H, $H^{o'}$), 8.01 (d, $J = 1.5$ Hz, 2H, H^5), 8.04 (t, J 7.8 Hz, 1H, $H^{4'}$), 8.25 (m, 4H, H^o), 8.73 (d, $J = 7.8$ Hz, 2H, $H^{3'}$), 8.88 (d, $J = 1.5$ Hz, 2H, H^3); ^{13}C NMR ($CDCl_3$, 61 MHz): $\delta = 117.8$ (2C), 118.5 (2C), 121.6 (2C), 127.1 (4C), 127.3 (4C), 128.8 (4C), 129.0 (1C), 129.05 (1C) 129.1 (4C), 137.8 (1C), 139.1 (2C), 139.5 (2C), 150.1 (2C), 155.5 (2C), 156.5 (2C), 157.2 (2C); IR (KBr): $\tilde{\nu} = 3061$m, 3034m, 1605m, 1577s, 1547s, 1497m, 1445w, 1391m, 820w, 759m, 689m, 642w, 616w cm^{-1}; EI-MS: *m/z*: 537 $[M^+]$; $C_{39}H_{27}N_3$ (537): elemental analysis calcd (%): C 87.1, H 5.1, N, 7.8; found: C 86.6, H 5.1, N 8.1.

6,6″-Dimethyl-2,2′:6′,2″-terpyridine (**5**): A mixture of **10** (200 mg, 0.57 mmol), **13** (320 mg, 1.2 mmol) and anhydrous ammonium acetate (3 g, excess) was heated at reflux in EtOH (10 mL) for 19 h. The reaction mixture was cooled, the solid filtered off and recrystallised from EtOH to give **5** as an off-white solid (94 mg, 63 %); m.p. > 250 °C; ^{1}H NMR ($CDCl_3$, 250 MHz): $\delta = 2.64$ (s, 6H, Me), 7.18 (d, $J = 7.3$ Hz, 2H, H^5), 7.73 (t, $J =$ 7.8 Hz, 2H, H^4), 7.89 (t, $J = 7.8$ Hz, 1H, $H^{4'}$), 8.40 (d, $J = 7.8$ Hz, 2H, H^3), 8.44 (d, $J = 7.8$ Hz, 2H, $H^{3'}$); ^{13}C NMR ($CDCl_3$, 61 MHz): $\delta = 24.7$ (2C), 118.2 (2C), 120.9 (2C), 123.3 (2C), 137.0 (2C), 137.8 (1C), 155.8 (4C), 157.9 (2C); IR (KBr): $\tilde{\nu} = 1570$m, 1437m, 1401s, 1077w, 995w, 779m, 635w cm^{-1}; TOF-MS: *m/z* : 261 $[M]^+$, 284 $[M+Na]^+$, 300 $[M+K]^+$.

6,6″Dimethyl-4,4′-diphenyl-2,2′:6′,2″-terpyridine (**6**): A mixture of **12** (0.18 g, 0.53 mmol), **13** (180 mg, 1.07 mmol) and anhydrous ammonium acetate (3 g, excess) was heated at reflux in ethanol (10 mL) for 19 h. The reaction mixture was cooled at 0 °C for 24 h before collecting the cream precipitate by filtration. Recrystallisation from ethanol gave **6** as an off-white solid (140 mg, 61 %); m.p. 239–240 °C; ^{1}H NMR ($CDCl_3$, 250 MHz): $\delta = 2.73$ (s, 6H, Me), 7.42–7.57 (m, 6H, H^m,H^p), 7.44 (d, $J = 1.4$ Hz, 2H, H^5), 7.78 (m, 4H, H^o), 7.98 (t, $J = 7.8$ Hz, 1H, $H^{4'}$), 8.51 (d, $J = 7.8$ Hz, 2H, $H^{3'}$), 8.69 (d, $J = 1.4$ Hz, 2H, H^3); ^{13}C NMR ($CDCl_3$, 61 MHz): $\delta = 24.8$ (2C), 116.6 (2C), 121.2 (4C), 127.2 (4C), 128.9 (2C), 129.0 (4C), 137.8 (2C), 138.9 (1C), 149.4 (2C), 155.7 (2C), 156.4 (2C), 158.4 (2C); IR (KBr): $\tilde{\nu} = 3032$m, 29119m, 1607m, 1576s, 1551s, 1497m, 1445m, 1391m, 1267w, 1077m, 1025w, 900w, 866w, 824m, 804w, 770s, 736w, 702m, 626m cm^{-1}; EI-MS: *m/z*: 413 $[M^+]$; $C_{29}H_{23}N_3$ (413); elemental analysis calcd: C 84.2, H, 5.6, N 10.2; found: C 83.7, H 5.6, N 10.2.

Iron complexes: general procedure: The ligand (20 mg) and $[NH_4]_2Fe(SO_4)_2 \cdot 6H_2O$ (0.5 molar equivalents) were heated to reflux in MeOH (20 mL) for the type 1 ligands or ethane-1,2-diol (10 mL) for the type 2 and type 3 ligands for 1 h. After cooling the mixture, an excess of a methanolic solution of $[NH_4](PF_6)$ was added, followed by water (10 mL), and the resulting solid filtered off and purified by column chromatography using silica gel as the matrix and MeCN/saturated aqueous KNO_3 solution/H_2O (14:2:1) as eluent. Further methanolic $[NH_4](PF_6)$ was added to the eluted purple or orange fraction, the MeCN removed in vacuo and the product isolated by filtration.

$[Fe(1)_2](PF_6)_2$: (purple solid) (0.028 g, 89 %). ^{1}H NMR (250 MHz, C_3D_6O): $\delta = -4.8$ (s, 1H, $H^{4'}$), 1.3 (s, 4H), 4.9 (s, 1H), 11.1 (s, 1H), 16.1 (s, 1H) 35.3 (s, 1H), 37.6 (s, 1H), 39.7 (s, 1H), 43.1 (s, 1H), 46.6 (s, 1H), 54.6 (s, 1H), 108.0 (s, 1H); $\tilde{\nu} = 1606$m, 1563m, 1461m, 1447m, 1242w, 842s, 766m, 700w, 556m cm^{-1}; UV/vis (CH_3CN): λ_{max} [nm] (ε [dm^3 mol^{-1}cm^{-1}]) = 230 (47000), 276 (36400), 324 (22000), 497 (sh), 549 (1400); TOFMS: *m/z*: 675 $[FeL_2]^+$, 384 $[FeLF]^+$, 365 $[FeL]^+$; elemental analysis calcd for $C_{42}H_{30}N_6FeP_2F_{12} \cdot 4H_2O$ (%): C 47.7, H 3.6, N 8.0; found: C 47.7, H 3.8, N 8.4.

$[Fe(2)_2](PF_6)_2$: purple solid (0.030 g, 92 %). ^{1}H NMR (250 MHz, C_3D_6O): $\delta = -2.8$, 8.4 (t ,$J = 7.4$ Hz, 2H, $H^{p'}$), 8.5 (t, $J = 7.4$ Hz, 4H, $H^{m'}$), 9.9 (d, $J =$ 7.4 Hz, 4H, $H^{m'}$), 15.1, 32.4, 34.7, 36.5, 38.8, 42.8, 49.9; $\tilde{\nu} = 1612$m, 1578w, 1544w, 1492w, 1462w, 1397w, 1242w, 1074w, 842s, 768m, 703m, 558m cm^{-1}; UV/vis (CH_3CN): λ_{max} [nm] (ε [dm^3 mol^{-1}cm^{-1}]): 248 (54200), 282 (44000), 335 (34500), 556 (4200); FABMS: *m/z*: 972 $[Fe(L_2)(PF_6)]^+$, 845 $[Fe(L_2)(F)]^+$, 826 $[Fe(L_2)]^+$, 460 $[Fe(L)F]^+$, 441 $[Fe(L)]^+$; elemental analysis calcd for $C_{54}H_{38}N_6FeP_2F_{12} \cdot H_2O$ (%): C 57.2, H 3.6, N 7.4; found: C 57.1, H 4.0, N 6.8.

$[Fe(3)_2](PF_6)_2$: (orange solid) (0.029 g, 88 %). ^{1}H NMR (250 MHz, C_3D_6O): $\delta = -20.4$ (s, 1H, $H^{4'}$), $-.3$ (br. s 2H, $H^{o/m/p}$), 0.6 (br. s 2H, $H^{o/m/p}$), 1.3 (4H, br. s, $H^{o/m/p}$), 4.1 (s, 2H, $H^{o/m/p}$), 14.4 (s, 2H, H^4), 58.6 (s, 2H, $H^{3/5}$), 67.7 (s, 2H, $H^{3'}$), 79.3 (s, 2H, $H^{3/5}$); $\tilde{\nu} = 1602$m, 1565m, 1484w, 1470m, 1449m, 1429m, 1243m, 1187w, 842s, 803m, 765m, 701m, 647w, 558m cm^{-1}; UV/vis (CH_3CN): λ_{max} [nm] (ε [dm^3 mol^{-1}cm^{-1}]) = 229 (56000), 304 (23000), 348 (16000); TOFMS: *m/z*: 605 $[FeL(PF_6)F]^+$, 460 $[FeLF]^+$, 441 $[FeL]^+$; elemental analysis calcd for $C_{54}H_{38}N_6FeP_2F_{12} \cdot 3H_2O$ (%): C 55.4, H 3.8, N 7.2; found: C 55.3, H 3.5, N 7.6.

$[Fe(4)_2](PF_6)_2$: (orange solid) (0.020 g, 76 %). ^{1}H NMR (250 MHz, C_3D_6O) δ -17.3 (s, 1H; $H^{4'}$), 1.2 (brs, 2H; $H^{o/m/p}$), 5.0 (s, 2H; $H^{o/m/p}$), 9.6 (s, 2H; $H^{p'}$), 10.0 (s, 4H; $H^{o'/m'}$) 13.4 (s, 4H; $H^{o'/m'}$), 59.7 (s, 2H; $H^{3/5}$), 69.6 (s, 2H; $H^{3'}$), 80.9 (s, 2H; $H^{3/5}$). $\tilde{\nu} = 1610$m, 1576m, 1544m, 1482m, 1387m, 1242w, 1973w, 840s, 763m, 670m, 558m cm^{-1}; UV/vis (CH_3CN): λ_{max} [nm] (ε [dm^3 mol^{-1}cm^{-1}]) = 248 (84000), 287 (47000), 343 (36000), 498 (sh); TOFMS: *m/z*: 1130 $[FeL_2]^+$, 593 $[FeL]^+$; elemental analysis calcd for $C_{78}H_{54}N_6FeP_2F_{12} \cdot H_2O$ (%): C 65.1, H 3.9, N 5.8; found: C 65.0, H 4.0, N 5.8.

$[Fe(5)_2](PF_6)_2$: (orange solid) (0.030g, 90 %). ^{1}H NMR (250 MHz, C_3D_6O): $\delta = -17.6$ (s, 1H, $H^{4'}$), -2.1 (s, 6H, Me), 9.7 (s, 2H, H^4), 53.7 (s, 2H, $H^{3/5}$), 57.8 (s, 2H, $H^{3/5}$), 69.1 (s, 2H, $H^{3'}$); $\tilde{\nu} = 1603$m, 1578w, 1479w, 1455m, 1383w, 1254w, 844s, 788m, 558m cm^{-1}; UV/vis (CH_3CN): λ_{max} [nm] (ε [dm^3 mol^{-1}cm^{-1}]) = 231 (47000), 273 (30000), 337 (27000); TOFMS: *m/z*: 577 $[FeL_2]^+$, 355 $[FeL(F)]^+$, 336 $[FeL]^+$.

$[Fe(6)_2](PF_6)_2$: (orange solid) (0.025 g, 88 %). ^{1}H NMR (250 MHz, C_3D_6O): $\delta = -13.9$ (s, 1H, $H^{4'}$), -2.4 (s, 6H, Me), 7.3 (t, 4H, $H^{o'/m'}$), 8.1 (t, 2H, $H^{p'}$), 9.0 (t, 4H, $H^{o'/m'}$), 51.9 (s, 2H, $H^{3/5}$), 56.9 (s, 2H, $H^{3/5}$), 69.5 (s, 2H, $H^{3'}$); $\tilde{\nu} =$ 1614m, 1575m, 1546m, 1453m, 842s, 766m, 696w, 631w, 558m cm^{-1}; UV/vis (CH_3CN): λ_{max} [nm] (ε [$dm^3 mol^{-1} cm^{-1}$]) = 248 (83500), 287 (46500), 343 (35500); TOFMS: *m/z*: 882 $[FeL_2]^+$, 488 $[FeL(PF_6)]^+$, 469 $[FeL]^+$.

Crystal structure analyses: The structures were solved by standard direct methods using standard techniques as indicated in Table 3. Crystallographic data (excluding structure factors) for the structures reported in this paper have been deposited with the Cambridge Crystallographic Data Center as supplementary publication no. CCDC-101409. Copies of the data can be obtained free of charge on application to CCDC, 12 Union Road, Cambridge CB21EZ, UK (fax: (+44) 1223-336-033; e-mail: deposit@ccdc.cam.ac.uk).

[1] P. Gütlich, A. Hauser, H. Spiering, *Angew. Chem.* **1994**, *106*, 2109; *Angew. Chem. Int. Ed. Engl.* **1994**, *33*, 2024.
[2] E. König, *Struct. Bonding* **1991**, *76*, 51.
[3] H. Toftlund, *Coord. Chem. Rev.* **1989**, *94*, 51.
[4] J. K. Beattie, *Adv. Inorg. Chem.* **1988**, *32*, 1.
[5] a) V.J Chen, A. M. Orville, M. R. Harpel, C. A. Frolik, K. K. Surerus, E. Münck, J. D. Lipscomb, *J. Biol. Chem.* **1989**, *264*, 21677; b) L.-J. Ming, L. Que, A. Kriauciunas, C. A. Frolik, V. Chen, *J. Biochem.*, **1991**, *30*, 11653; c) C. R. Randall, Y. Zang, A. E. True, L. Que, J. M. Charnock, C. D. Garner, Y. Fujishima, C. J. Schofield, J. E. Baldwin, *Biochem.* **1993,** *32*, 6664; d) Y. Zang, L. Que, *Inorg. Chem.* **1995**, *34*, 1030.
[6] M. A. Holmes, I. L. Trong, S. Turley, L. C. Sieker, R. E. Stenkamp, *J Mol. Biol.* **1991**, *218*, 583.
[7] P. Nordlund, B.-M. Sjöberg, H. Eklund, *Nature (London)*, **1990**, *345*, 593.
[8] a) S. Sugden, *J. Chem. Soc.* **1943**, 3570; b) F. H. Burstall, R. S. Nyholm, *J. Chem. Soc.* **1952**, 3570; c) W. W. Brandt, F. P. Dwyer, E. C. Gyarfas, *Chem. Rev.* **1954**, *54*, 959; d) H. Irving, D. H. Mellor, *J. Chem. Soc.* **1962**, 5222; e) J. F. Duncan, K. F. Mok, *J. Chem. Soc.* **1966**, 1493.
[9] a) H. Irving, M. J. Mellor, *J. Chem. Soc.* **1962**, 5237; b) H. A. Goodwin, R. N. Sylva, *Aust. J. Chem.* **1968**, *21*, 83; c) J. Fleisch, P. Gütlich, K. M. Hasselbach, W. Müller, *Inorg. Chem.* **1976**, *15*, 958; d) E. König, H. Spiering, S. Kremer, K. Madeja, A. Rosenkranz, *J. Chem. Phys.* **1972**, *56*, 3139.
[10] L. J. Charbonnière, A. F. Williams, C. Piguet, G. Bernardinelli, E. Rivara-Minten, *Chem. Eur. J.* **1998**, *4*, 485.
[11] C. Piguet, E. Rivara-Minten, G. Bernardinelli, J.-C. G. Bünzli, G. Hopfgartner, *J. Chem. Soc. Dalton Trans.* **1997**, 421.
[12] E. C. Constable, M. D. Ward, *Inorg. Chim. Acta* **1988**, *141*, 201.
[13] a) E. C. Constable, A. M. W. Cargill Thompson, *J. Chem. Soc. Dalton Trans.* **1992**, 2947; b) E. C. Constable, D. R. Smith, *Supramol. Chem.*, **1994,** *4*, 5.
[14] R. Chotalia, E. C. Constable, M. Neuburger, D. R. Smith, M. Zehnder, *J. Chem. Soc. Dalton Trans.* **1996**, 4207.
[15] F. Kröhnke, *Synthesis* **1976**, 1.
[16] E. C. Constable, F. Heirtzler, M. Neuburger, M. Zehnder, *J. Am. Chem. Soc.* **1997**, *119*, 5606.
[17] C. O. Dietrich-Buchecker, P. A. Marnot, J.-P. Sauvage, *Tetrahedron Lett.* **1982**, 5291.
[18] I. Bertini, C. Luchinat, *Coord. Chem. Revs.* **1996**, *150*, 1.
[19] E. C. Constable, T. Kulke, M. Neuburger, M. Zehnder, *New J. Chem.* **1997**, *21*, 1091.
[20] a) P. Bugnon, J.-C. Chottard, J.-L. Jestin, B. Jung, G. Laurenczy, M. Maeder, A. Merbach, A. D. Zuberbühler, *Anal. Chim. Acta* **1994**, *298*, 195; b) R. M. Dyson, S. Kaderli, G. A. Lawrance, M. Maeder, A. D. Zuberbühler, *Anal. Chim. Acta* **1997**, *353*, 381.
[21] P. Adler, H. Spiering, P. Gütlich, *Inorg. Chem.* **1987**, *26*, 3840.
[22] J. J. McGarvey, I. Lawthers, K. Heremans, H. Toftlund, *J. Chem. Soc. Chem. Commun.* **1984**, 1575.
[23] J. Dibenedetto, V. Arkle, H. A. Goodwin, P. C. Ford, *Inorg. Chem.* **1985**, *24*, 455.
[24] J. J. McGarvey, I. Lawthers, K. Heremans, H. Toftlund, *Inorg. Chem.* **1990**, *29*, 252.
[25] A.T Baker, H,A. Goodwin, *Aust. J. Chem.* **1985**, *38*, 207.
[26] P. Laine, A. Gourdon, J.-P. Launay, *Inorg.Chem.* **1995**, *34*, 5156.
[27] E. C. Constable, J. E. Davies, D. Phillips, P. R. Raithby, *Polyhedron* **1998**, *17*, 3989.
[28] M. Spitzer, F. Gartig, R. van Eldik, *Rev. Sci. Instrum.* **1988**, *59*, 2092.
[29] C. L. Beswick, R. D. Shalders, T. W. Swaddle, *Inorg. Chem.* **1996**, *35*, 991.
[30] E. C. Constable, J. Lewis, *Polyhedron* **1982**, *1*, 303.

Received: June 12, 1998
Revised version: September 23 [F1203]